

Discovery of Mafic Granulites in the Muzhaerte Area, SW Tianshan, China

Jun Yan ¹, Ying Cui ^{1,*} and Xiaoyu Liu ^{2,*}

¹ MOE Key Laboratory of Orogenic Belt and Crustal Evolution, School of Earth and Space Sciences, Peking University, Beijing 100871, China; 2201110641@pku.edu.cn

² National Research Center for Geoanalysis, Beijing 100037, China

* Correspondence: cy0430@pku.edu.cn (Y.C.); liuxiaoyu0725@163.com (X.L.)

Abstract: Accretionary and collisional orogeny are often accompanied by the disturbance of the geothermal gradient, leading to high-temperature metamorphism. High-temperature metamorphic rocks are significant in their ability to help the reconstruction of the thermal histories of orogenic belts. The Tianshan Orogenic Belt, at the southwest margin of the Central Asian Orogenic Belt, is a record of the long-term subduction–collision–post-collision orogenic process that has taken place in the Phanerozoic Eon. Here, we report the discovery of mafic granulites in the Muzhaerte area, SW Tianshan. Petrographic observation reveals that the mafic granulites underwent two metamorphic stages. The peak mineral assemblage of the first stage is dominated by clinopyroxene + orthopyroxene + plagioclase + quartz + hornblende (hb¹) ± biotite, and the post-peak mineral assemblage of the second stage is dominated by clinopyroxene + plagioclase + quartz + hornblende (hb²) + biotite. The calculated results obtained from the two-pyroxene thermobarometers and the Al-in-hornblende barometer for the mafic granulites indicate that the metamorphic conditions of mafic granulites are 760–860 °C, <0.39–0.41 Gpa. The mafic granulites recorded a high-grade granulite facies thermal metamorphic event with the highest temperature limit currently recorded in the Central Tianshan Block.

Keywords: mafic granulites; Tianshan; Muzhaerte; high-temperature metamorphism; geothermobarometry



Citation: Yan, J.; Cui, Y.; Liu, X.

Discovery of Mafic Granulites in the Muzhaerte Area, SW Tianshan, China. *Minerals* **2023**, *13*, 1214. <https://doi.org/10.3390/min13091214>

Academic Editor: Giorgio Garuti

Received: 23 August 2023

Revised: 6 September 2023

Accepted: 13 September 2023

Published: 15 September 2023



Copyright: © 2023 by the authors. Licensee MDPI, Basel, Switzerland. This article is an open access article distributed under the terms and conditions of the Creative Commons Attribution (CC BY) license (<https://creativecommons.org/licenses/by/4.0/>).

1. Introduction

In plate tectonics, accretionary orogeny and collisional orogeny are often accompanied by the disturbance of the geothermal gradient, which leads to high-temperature metamorphism and the partial melting of crustal rocks [1–3]. High-temperature metamorphism and the partial melting of crustal rocks may lead to changes in the rock constitution, rock chemical composition, and rheological properties of the lithosphere [4–6]. High-temperature metamorphic rocks are significant in their ability to reconstruct the thermal histories of orogenic belts.

The South Tianshan Orogenic Belt (STOB) is a Paleozoic subduction–collision orogenic belt located in the southwest margin of the Central Asian Orogenic Belt (CAOB) [7,8]. As a key area of the Central Asian Orogenic Belt, the South Tianshan Orogenic Belt completely preserves the whole process from the regeneration of the oceanic crust to the continent–continent collision orogeny, and provides an excellent region for studying the tectonic evolution of the southwest Central Asian Orogenic Belt [7,8]. It was formed via the subduction of the South Tianshan Ocean (STO) into the northern Yili-Central Tianshan Block (YCTB), and the collision of the Tarim Craton with the YCTB after the closure of the oceanic crust [9,10]. Continuous subduction and collision resulted in a large number of ophiolite fragments, accretionary complexes, island arc migmatites and ultrahigh-high-pressure metamorphic rocks in the STOB and the YCTB [11–16]. In recent decades, in-depth research has been carried out on these rocks, and the tectonic evolutionary history

of the STOB has been determined [17–19]. The STO opened in the Neoproterozoic era and began to subduct into the YCTB in the Early Paleozoic Era [16,20–23]. The closure of the STO occurred in the late Early Carboniferous period; then, syn- and post-collision magmatism occurred in the Tianshan Orogenic Belt [24–27]. The reported high-temperature metamorphic rocks in this orogenic belt consist of amphibolites, granitic and pelitic gneisses, with minor amounts of mafic granulites, which are assumed to be major constituents of the crystalline basement of Central Tianshan [7,28,29]. Their peak temperatures are ~ 700 °C, they are close to wet, and they possess the minimum melting conditions of supracrustal rocks, which are common during arc crust reworking [14,30,31]. It is unknown whether they represent the upper temperature limit during the evolution of the Central Tianshan arc. Herein, we report the discovery of orthopyroxene-bearing mafic granulites in the south of the Muzhaerte area, SW Tianshan Orogenic Belt. We conducted petrography observations and geothermobarometry calculations on mafic granulites and determined that the metamorphic conditions of granulites are 760–860 °C and <0.39–0.41 GPa. The mafic granulites recorded a higher heat flow compared to previously reported metamorphic rocks in the Central Tianshan Block.

2. Geological Setting

The Tianshan Orogenic Belt, sandwiched between the Yili-Kazakhstan Plate and the Tarim Craton, is an important part of the CAO, which has experienced a long and complex process of accretion and orogeny [8,20,32]. From north to south, the Tianshan Orogenic Belt in China can be divided into the North Tianshan Orogenic Belt, the YCTB and the STOB [25,33]. Mid-ocean ridge basalts representing the Terskey Ocean crust have been found in the Nalati northern margin fault of the YCTB, so the YCTB is further divided into the Yili Block (YB) and the Central Tianshan Block (CTB) [34].

The formation of the North Tianshan Orogenic Belt (NTOB) is related to the southward subduction of the North Tianshan Ocean (NTO) into the YB [7,35]. A large number of ophiolite and arc magmatic rocks associated with subduction are exposed in the NTOB and the northern margin of the YB [36,37]. The NTOB and the YB are separated by the North Tianshan Fault. The boundary between the YB and the CTB is the Nalati north margin fault, which is considered to be connected with the Nikolayev line in Kyrgyzstan [20,34,38]. The formation of the STOB is related to the northward subduction of the STO into the CTB [32,39–41]. A large number of ophiolites, arc magmatic rocks and ultrahigh-high-pressure metamorphic rocks related to subduction are exposed in the STOB, the CTB and the southern margin of the YB [12,42–44]. The STOB and the YB are separated by the South Central Tianshan Fault.

The Muzhaerte area (near the Muzhaerte River) is located at the south margin of the CTB and the north edge of the South Central Tianshan Fault (Figure 1). The CTB is a long and narrow terrain with a Precambrian crystalline basement between the YB and the STOB [45]. The Precambrian crystalline basement includes Neoproterozoic metamorphic granitoid and mafic rock, amphibolite, migmatite, biotite plagioclase gneiss, metamorphic clastic rock and carbonate rock [46,47]. There were many magmatic rocks of island arc produced by the subduction of the STO, as well as many high-temperature metamorphic rocks related to the arc magmatism of the Early Paleozoic Era [48–50]. The pre-Carboniferous magmatic rocks and strata were subjected to deformation and greenschist–amphibolite facies metamorphism grades [51,52]. After the collision between the Tarim Craton and the YCTB, some Permian magmatic rocks also appeared in the CTB under the tense post-collision environment [26,48]. The Muzhaerte area on the north side of the South Central Tianshan Fault is considered as a high-temperature metamorphic belt, while the area on the south side of the fault is considered as an ultrahigh/high-pressure metamorphic belt, forming a contrasting paired metamorphic belt [43]. The peak metamorphic conditions obtained from the previous studies of pelitic granulites in this area are 630–705 °C, 0.47–0.58 GPa [30,31]. The main lithology of the ultrahigh/high-pressure metamorphic belt is interbedded and lenticular muscovite schist, blueschist and eclogite [28,53]. Accord-

ing to the summary of the P-T path of published ultrahigh/high-pressure metamorphic rock, the peak metamorphic conditions of metamorphic rock have been estimated to be 430–510 °C, 2.2–3.3 Gpa [13,53,54]. The U-Pb ages of zircons from eclogite and muscovite schist containing coesite are ~320 Ma, which represents the final time of collision between Tarim Craton and the CTB [20,21,43]. The metamorphic rocks in two metamorphic belts show disparate geothermal gradients.

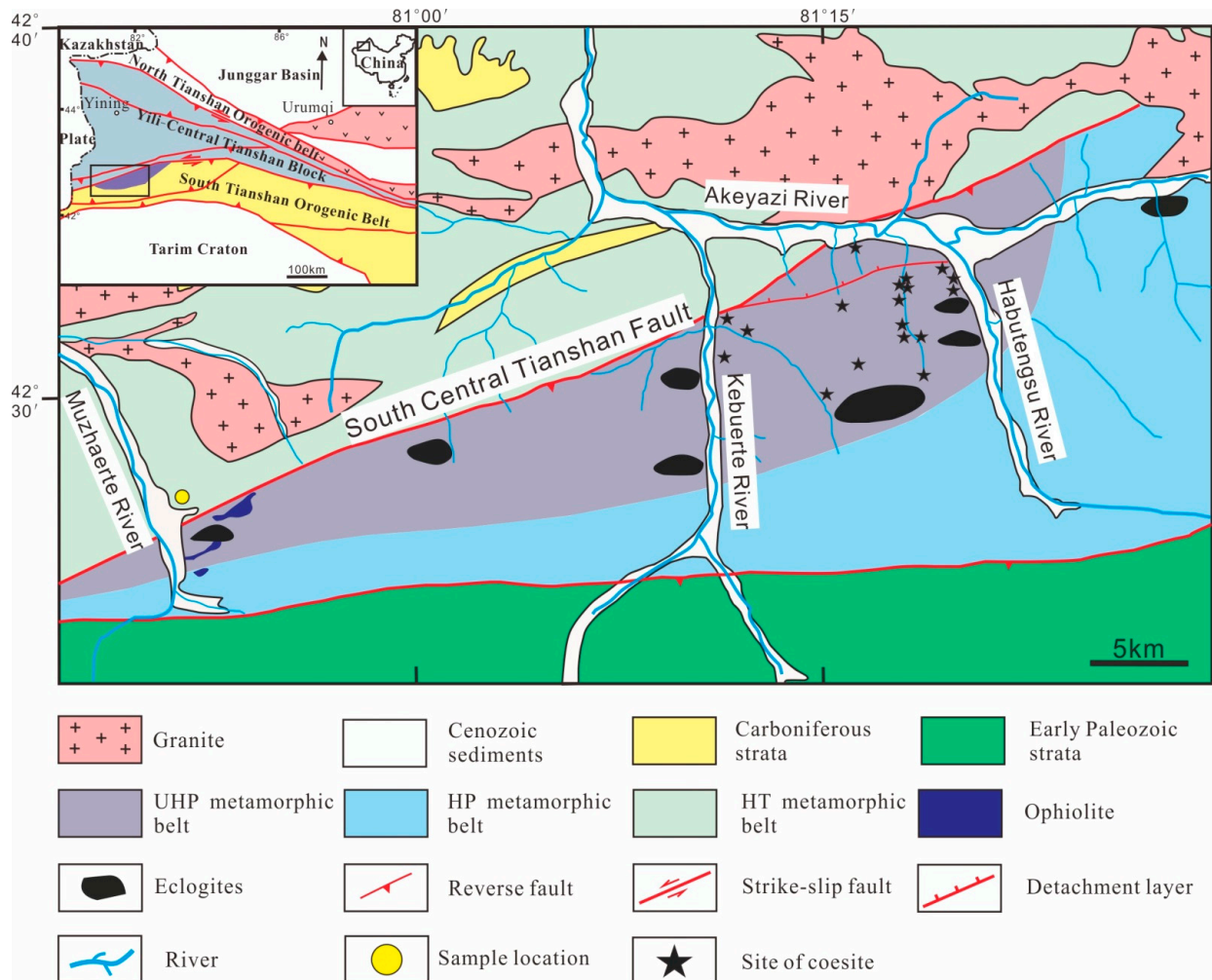


Figure 1. Geological structure sketch of the Muzhaerte area, geological sketch and sampling location (modified after [43,48]).

3. Materials and Methods

The mafic granulites were collected from the east of the Muzhaerte River, in the high-temperature metamorphic belt of the Central Tianshan Block. The studied granulites consist of plagioclase, clinopyroxene, orthopyroxene, hornblende, quartz and biotite, with accessory apatite and ilmenite. They are massive, showing typical granoblastic textures (Figure 2a). Both clinopyroxene and orthopyroxene are anhedral, with grain sizes ranging from 0.1 to 0.5 mm (Figure 2b), and are mostly surrounded by hornblende (Figure 2c). Most of the clinopyroxene occurs as porphyroblasts, containing biotite, hornblende inclusions (Figure 2d). Some of the clinopyroxene develops oriented orthopyroxene rods along the c-axis (Figure 2e). Orthopyroxene occurs as relict individual grains or as intergrowth with clinopyroxene. Hornblende can be divided into two sub-types based on morphology. In the first type, the hornblende (hb^1) occurs as inclusions in the pyroxenes or shows granoblastic texture with pyroxene. This indicates that this type of hornblende is intergrown with pyroxene. Some hornblende grains are small and round, and occur as residues of prograde

dehydration melting during progressive metamorphism. Part of these grains have cusped boundaries, which represent the growth during the later cooling process. The other type of hornblende (hb^2) is formed at the rim of pyroxene, or in the form of huge grains that contain some anhydrous inclusions (pyroxene and plagioclase), indicating that it was formed in the retrogressive metamorphic process (Figure 2f). Plagioclase and quartz are subhedral to anhedral and have grain sizes of 0.2–0.4 mm. Biotite is mostly distributed around anhydrous pyroxene or amphibole.

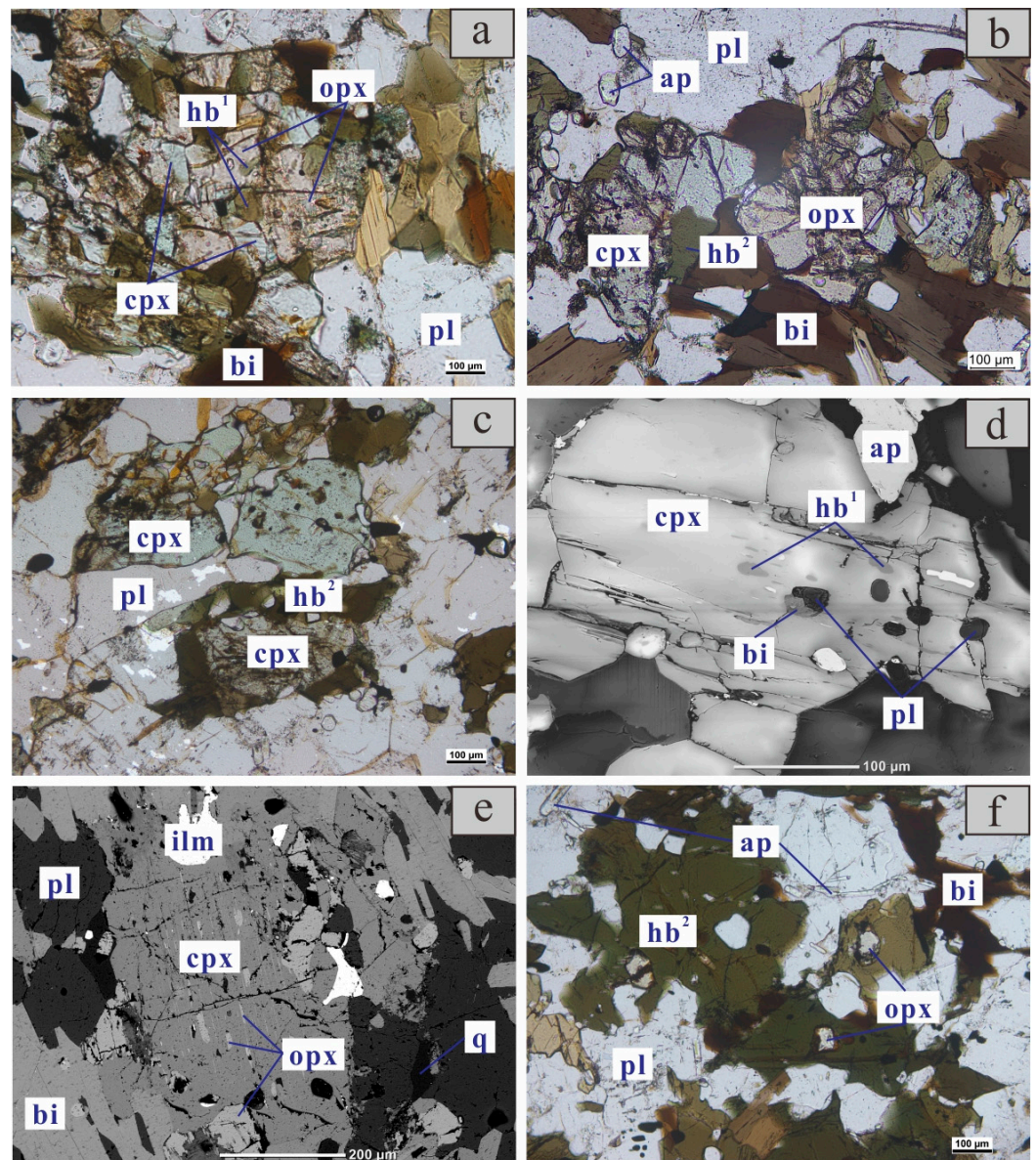


Figure 2. Photomicrographs of the mafic granulites in the Muzhaerte area. (a) Equigranular granoblastic texture of granulites (taken in plane polarized light). (b) Anhedral crystal forms of the two pyroxenes (taken in plane polarized light). (c) Two pyroxenes have retrogressive amphibole reaction rims (taken in plane polarized light). (d) The clinopyroxene occurs as rounded porphyroblasts, containing biotite, hornblende and plagioclase inclusions (backscatter photo by JCM-6000PLUS). (e) Clinopyroxene develops oriented orthopyroxene rods along the c-axis (backscatter photo by JCM-6000PLUS). (f) The hornblende (hb^2) formed at the rim of pyroxene or in the form of huge grains that contain some anhydrous inclusions (taken in plane polarized light). Mineral code: cpx—clinopyroxene; opx—orthopyroxene; hb—hornblende; bi—biotite; pl—plagioclase; q—quartz; ap—apatite; ilm—ilmenite.

The textures show that the Muzhaerte mafic granulites underwent at least two metamorphic stages of peak and post-peak metamorphism (Figure 3). During prograde metamorphism, hornblende is decomposed to form clinopyroxene, orthopyroxene and plagioclase, whereas the other hornblende maintains stability, shown by its rounded occurrences in the matrix or as inclusions in pyroxene. Thus, the peak mineral assemblage is clinopyroxene + orthopyroxene + plagioclase + quartz + hornblende (hb^1) ± biotite (Phase I). During cooling, the unmigrated melt reacts with clinopyroxene, orthopyroxene and plagioclase or pyroxene hydrates in an aqueous fluid phase to form the hydrous mineral amphibole. Therefore, amphibole grows along the rim of pyroxene or early-stage amphibole. The mineral assemblage of the post-peak stage is clinopyroxene + plagioclase + quartz + hornblende (hb^2) + biotite (Phase II). The absence of garnet and rutile indicates that the Muzhaerte mafic granulites were formed at medium to low pressures.

The determination of the metamorphic conditions of mafic granulites has generally relied on conventional geothermobarometry. Two-pyroxene thermobarometers are often used to calculate the metamorphic temperature conditions of mafic granulites. The principle of thermometers is based on the molar ratio relationship between the Fe and Mg ions in the exchange reaction between clinopyroxene and orthopyroxene, in order to restore the temperature at which the mineral combination is stable [55–57]. The typical thermobarometers used currently include three versions established by Wood [57], Wells [56] and Brey [55]. Wood [40] proposed an empirical formula for calculating the equilibrium temperature of two-pyroxene assemblages by considering Fe^{2+} in the miscibility gap between two pyroxenes [57]. Wells [39] used most of the available experimental data for multi-component pyroxene to calibrate a two-pyroxene thermobarometer [56]. Brey [38] evaluated the original thermobarometer based on the experimental data of the four-phase Lherzolite and developed a new version of the thermobarometer, which is relatively more suitable for higher-temperature and -pressure conditions [55].

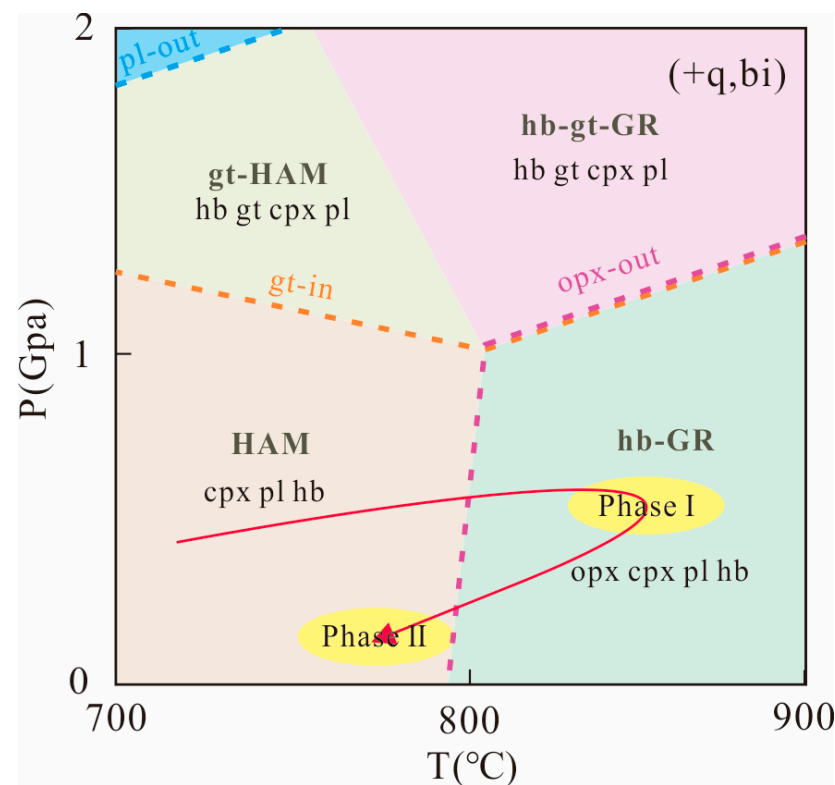


Figure 3. Conjectural metamorphic P-T trajectory of the mafic granulites in the Muzhaerte area (modified after [58]). The mafic granulites underwent at least two metamorphic stages of peak and post-peak metamorphism. Metamorphic facies code: GR—granulite facies; HAM: high-amphibolite facies.

At present, it is difficult to accurately constrain the pressure of the mafic granulites, so an Al-in-hornblende barometer is selected to roughly evaluate the pressure condition. The Al-in-hornblende barometer calculates the pressure based on the Al content in hornblende [59–61]. Although the barometer has been proposed for using in magmatic rocks, it is also suitable for metamorphic rocks when the pressure range is 0.2–1.3 Gpa and the rock contains mineral combinations of quartz/alkali-feldspar, plagioclase, hornblende, biotite and Fe-Ti-oxide [50]. However, the correlation between the pressure and temperature of the system implies that the temperature will also affect the calculation of the pressure. Therefore, we selected Anderson's [50] version of the Al-in-hornblende barometer with temperature correction, and Hammarstrom's [51] and Schmidt's [52] version without temperature correction for the pressure calculation.

4. Results and Discussion

The calculated results for the two-pyroxene thermobarometers and the Al-in-hornblende barometers are listed in Supplementary Tables S1 and S2. The temperature range calculated according to the Wood [40] thermobarometer is 762–811 °C, with an average temperature of 789 °C. The temperature range calculated according to the Wells [39] thermobarometer is 785–860 °C, with an average temperature of 829 °C. The temperature range calculated according to the Brey [38] thermobarometer is 533–632 °C, with an average temperature of 590 °C. The pressure ranges calculated based on the Anderson [42] barometer are 0.35–0.37 Gpa and 0.39–0.41 Gpa at the given temperatures of 780 °C and 760 °C. As the given temperature increases, the calculated pressure result will decrease. The pressure range calculated based on the Hammarstrom [43] barometer is 0.49–0.51 Gpa. The pressure range calculated based on the Schmidt [44] barometer is 0.53–0.55 Gpa.

The calculation results of the Brey thermobarometer are significantly lower than those of the other two thermobarometers. This may be because the Brey thermobarometer results are obtained using lherzolite samples under higher temperatures and pressures, so it is not suitable for analyzing mafic granulites. The calculation results of the Anderson barometer are significantly lower than those of the other two versions, indicating that neglecting the influence of temperature will result in an overestimation of the calculation result for pressure. Therefore, we preliminarily believe that the metamorphic conditions of mafic granulites are 760–860 °C and <0.39–0.41 Gpa.

The discovered Muzhaerte mafic granulites record the high-temperature granulite facies metamorphism of the CTB. The associated meta-sedimentary rocks and pelitic gneiss (Cordierite garnet sillimanite gneiss) in the adjacent area also record high-temperature metamorphism [14,31,48]. Phase equilibrium modeling shows that the peak metamorphic conditions of the meta-sedimentary rocks and pelitic gneiss are 728 °C and 0.72 Gpa, and 681–705 °C and 0.54–0.58 Gpa, respectively. This suggests that the mafic granulites examined in the study are able to record a higher heat flow and the highest peak temperature in the CTB found so far. The mafic granulites may represent the Precambrian basement of the CTB or form in the continental arc environment during oceanic subduction or the post-collisional extensional environment. At present, there are no geochronology data available with which to judge the tectonic background of granulite formation, but their higher peak temperature and lower peak pressure may suggest that they may have been formed in a shallower tensile environment and unrelated to continental arc magmatism. Considering that the Tianshan Orogenic Belt was in a post-collision environment with intraplate magmatic rocks in the Permian period, the granulite facies metamorphism may have occurred in a post-collision environment presumably, under the condition that the thinning of the crust and asthenosphere upwelling provided heat [25].

5. Conclusions

1. The Muzhaerte mafic granulites underwent two metamorphic stages, the first being the peak mineral assemblage of clinopyroxene + orthopyroxene + plagioclase + quartz

- + hornblende (hb¹) ± biotite, and the second being the post-peak mineral assemblage of clinopyroxene + plagioclase + quartz + hornblende (hb²) + biotite.
- Using the two-pyroxene thermobarometers and the Al-in-hornblende barometer, the metamorphic conditions of the mafic granulites were determined to be 760–860 °C, and <0.39–0.41 Gpa. This recorded a high-grade granulite facies thermal metamorphic event with the highest temperature limit currently recorded in the CTB.

Supplementary Materials: The following supporting information can be downloaded at: <https://www.mdpi.com/article/10.3390/min13091214/s1>, Table S1: The calculated results obtained for the mafic granulites in the Muzhaerte using the two-pyroxene thermobarometers; Table S2: The calculated results obtained for the mafic granulites in the Muzhaerte using the Al-in-hornblende barometers.

Author Contributions: Conceptualization, J.Y. and Y.C.; methodology, J.Y.; software, J.Y.; formal analysis, J.Y.; investigation, J.Y. and Y.C.; resources, J.Y. and Y.C.; data curation, J.Y.; writing—original draft preparation, J.Y.; writing—review and editing, J.Y., X.L. and Y.C. All authors have read and agreed to the published version of the manuscript.

Funding: This research was funded by China National Petroleum Corporation-Peking University Strategic Cooperation Project of Fundamental Research. The funder of the project is named Zhang Lifei.

Data Availability Statement: The data that support the findings of this study are available from the corresponding author, Ying Cui, upon reasonable request.

Acknowledgments: We are also grateful to Lv Zeng for his assistance.

Conflicts of Interest: The authors declare no conflict of interest.

References

- Brown, M. Orogeny, migmatites and leucogranites: A review. *J. Earth Syst. Sci.* **2001**, *110*, 313–336. [[CrossRef](#)]
- Stuart, C.A.; Daczko, N.R.; Piazzolo, S. Local partial melting of the lower crust triggered by hydration through melt-rock interaction: An example from Fiordland, New Zealand. *J. Metamorph. Geol.* **2017**, *35*, 213–230. [[CrossRef](#)]
- Whittington, A.G.; Treloar, P.J. Crustal anatexis and its relation to the exhumation of collisional orogenic belts, with particular reference to the Himalaya. *Mineral. Mag.* **2002**, *66*, 53–91. [[CrossRef](#)]
- Brown, M. Crustal melting and melt extraction, ascent and emplacement in orogens: Mechanisms and consequences. *J. Geol. Soc. Lond.* **2007**, *164*, 709–739. [[CrossRef](#)]
- Brown, M. Granite: From genesis to emplacement. *Geol. Soc. Am. Bull.* **2013**, *125*, 1079–1113. [[CrossRef](#)]
- Vanderhaeghe, O.; Teyssier, C. Crustal-scale rheological transitions during late-orogenic collapse. *Tectonophysics* **2001**, *335*, 211–228. [[CrossRef](#)]
- Gao, J.; Maosong, L.; Xuchang, X.; Yaoqing, T.; Guoqi, H. Paleozoic tectonic evolution of the Tianshan Orogen, northwestern China. *Tectonophysics* **1998**, *287*, 213–231. [[CrossRef](#)]
- Xiao, W.; Santosh, M. The western Central Asian Orogenic Belt: A window to accretionary orogenesis and continental growth. *Gondwana Res.* **2014**, *25*, 1429–1444. [[CrossRef](#)]
- Windley, B.F.; Alexeiev, D.V.; Xiao, W.; Kröner, A.; Badarch, G. Tectonic models for accretion of the Central Asian Orogenic Belt. *J. Geol. Soc.* **2007**, *164*, 31–47. [[CrossRef](#)]
- Xiao, W.; Windley, B.F.; Allen, M.B.; Han, C. Paleozoic multiple accretionary and collisional tectonics of the Chinese Tianshan orogenic collage. *Gondwana Res.* **2013**, *23*, 1316–1341. [[CrossRef](#)]
- Gou, L.-L.; Zhang, L.-F. Geochronology and petrogenesis of granitoids and associated mafic enclaves from Xiata in Chinese Southwest Tianshan: Implications for early Paleozoic tectonic evolution. *J. Asian Earth Sci.* **2016**, *115*, 40–61. [[CrossRef](#)]
- Jiang, T.; Gao, J.; Klemd, R.; Qian, Q.; Zhang, X.; Xiong, X.; Wang, X.; Tan, Z.; Chen, B. Paleozoic ophiolitic mélanges from the South Tianshan Orogen, NW China: Geological, geochemical and geochronological implications for the geodynamic setting. *Tectonophysics* **2014**, *612–613*, 106–127. [[CrossRef](#)]
- Lü, Z.; Bucher, K. The coherent ultrahigh-pressure terrane of the Tianshan meta-ophiolite belt, NW China. *Lithos* **2018**, *314–315*, 260–273. [[CrossRef](#)]
- Xia, B.; Zhang, L.; Bader, T. Zircon U–Pb ages and Hf isotopic analyses of migmatite from the ‘paired metamorphic belt’ in Chinese SW Tianshan: Constraints on partial melting associated with orogeny. *Lithos* **2014**, *192–195*, 158–179. [[CrossRef](#)]
- Zhang, L.; Zhang, L.; Xia, B.; Lü, Z. Metamorphic P–T path and zircon U–Pb dating of HP mafic granulites in the Yushugou granulite-peridotite complex, Chinese South Tianshan, NW China. *J. Asian Earth Sci.* **2018**, *153*, 346–364. [[CrossRef](#)]

16. Zhao, L.; Chen, H.; Han, J.; Jiao, J. Paleozoic tectonic setting and evolution of the Central Tianshan Block: Insights from Devonian arc-related granitoids. *J. Asian Earth Sci.* **2022**, *239*, 105402. [[CrossRef](#)]
17. Tao, Z.; Yin, J.; Sun, M.; Wang, T.; Yuan, C.; Chen, W.; Huang, H.; Seltmann, R.; Thomson, S.N.; Chen, Y. Spatial and temporal variations of geochemical and isotopic compositions of Paleozoic magmatic rocks in the Western Tianshan, NW China: A magmatic response of the Advancing and Retreating Subduction. *J. Asian Earth Sci.* **2022**, *232*, 105112. [[CrossRef](#)]
18. Su, W.; Cai, K.; Sun, M.; Wan, B.; Wang, X.; Bao, Z.; Xiao, W. Carboniferous volcanic rocks associated with back-arc extension in the western Chinese Tianshan, NW China: Insight from temporal-spatial character, petrogenesis and tectonic significance. *Lithos* **2018**, *310–311*, 241–254. [[CrossRef](#)]
19. Huang, H.; Wang, T.; Tong, Y.; Qin, Q.; Ma, X.; Yin, J. Rejuvenation of ancient micro-continents during accretionary orogenesis: Insights from the Yili Block and adjacent regions of the SW Central Asian Orogenic Belt. *Earth-Sci. Rev.* **2020**, *208*, 103255. [[CrossRef](#)]
20. Gao, J.; Long, L.; Klemm, R.; Qian, Q.; Liu, D.; Xiong, X.; Su, W.; Liu, W.; Wang, Y.; Yang, F. Tectonic evolution of the South Tianshan orogen and adjacent regions, NW China: Geochemical and age constraints of granitoid rocks. *Int. J. Earth Sci.* **2008**, *98*, 1221–1238. [[CrossRef](#)]
21. Klemm, R.; John, T.; Scherer, E.E.; Rondenay, S.; Gao, J. Changes in dip of subducted slabs at depth: Petrological and geochronological evidence from HP–UHP rocks (Tianshan, NW-China). *Earth Planet. Sci. Lett.* **2011**, *310*, 9–20. [[CrossRef](#)]
22. Zhang, H.; Zhu, Y.; Feng, W.; Tan, Y.; An, F.; Zheng, J. Paleozoic intrusive rocks in the Nalati mountain range (NMR), southwest Tianshan: Geodynamic evolution based on petrology and geochemical studies. *J. Earth Sci.* **2017**, *28*, 196–217. [[CrossRef](#)]
23. Wang, X.-S.; Klemm, R.; Gao, J.; Jiang, T.; Li, J.-L.; Xue, S.-C. Final Assembly of the Southwestern Central Asian Orogenic Belt as Constrained by the Evolution of the South Tianshan Orogen: Links with Gondwana and Pangea. *J. Geophys. Res. Solid Earth* **2018**, *123*, 7361–7388. [[CrossRef](#)]
24. Gou, L.-L.; Zhang, L.-F.; Tao, R.-B.; Du, J.-X. A geochemical study of syn-subduction and post-collisional granitoids at Muzhaerte River in the Southwest Tianshan UHP belt, NW China. *Lithos* **2012**, *136–139*, 201–224. [[CrossRef](#)]
25. Han, B.-F.; He, G.-Q.; Wang, X.-C.; Guo, Z.-J. Late Carboniferous collision between the Tarim and Kazakhstan–Yili terranes in the western segment of the South Tian Shan Orogen, Central Asia, and implications for the Northern Xinjiang, western China. *Earth-Sci. Rev.* **2011**, *109*, 74–93. [[CrossRef](#)]
26. Cheng, Z.; Zhang, Z.; Santosh, M.; Zhao, Z.; Chen, L. Late Carboniferous to early Permian partial melting of the metasedimentary rocks and crustal reworking in the Central Asian Orogenic Belt: Evidence from garnet-bearing rhyolites in the Chinese South Tianshan. *Lithos* **2017**, *282–283*, 373–387. [[CrossRef](#)]
27. Yin, J.; Chen, W.; Hodges, K.V.; Xiao, W.; Cai, K.; Yuan, C.; Sun, M.; Liu, L.-P.; van Soest, M.C. The thermal evolution of Chinese central Tianshan and its implications: Insights from multi-method chronometry. *Tectonophysics* **2018**, *722*, 536–548. [[CrossRef](#)]
28. Gao, J.; Klemm, R.; Zhang, L.; Wang, Z.; Xiao, X. P–T path of high-pressure/low-temperature rocks and tectonic implications in the western Tianshan Mountains, NW China. *J. Metamorph. Geol.* **1999**, *17*, 621–636. [[CrossRef](#)]
29. Wang, X.-S.; Gao, J.; Klemm, R.; Jiang, T.; Li, J.-L.; Zhang, X.; Xue, S.-C. The Central Tianshan Block: A microcontinent with a Neoproterozoic–Paleoproterozoic basement in the southwestern Central Asian Orogenic Belt. *Precambrian Res.* **2017**, *295*, 130–150. [[CrossRef](#)]
30. Gou, L.; Zhang, L. Petrology and U-Th-Pb chemical monazite dating of the low-P metapelitic granulites at the region of Muzhaerte River in southwestern Tianshan, NW China, and their geological implications. *Acta Petrol. Sin.* **2009**, *25*, 2271–2280.
31. Li, Q.; Zhang, L. The P-T path and geological significance of low-pressure granulite-facies metamorphism in Muzhaerte, southwest Tianshan. *Acta Petrol. Sin.* **2004**, *20*, 583–594.
32. Allen, M.B.; Windley, B.F.; Zhang, C. Palaeozoic collisional tectonics and magmatism of the Chinese Tien Shan, central Asia. *Tectonophysics* **1992**, *220*, 89–115. [[CrossRef](#)]
33. Biske, Y.S.; Seltmann, R. Paleozoic Tian-Shan as a transitional region between the Rheic and Urals-Turkestan oceans. *Gondwana Res.* **2010**, *17*, 602–613. [[CrossRef](#)]
34. Qian, Q.; Gao, J.; Klemm, R.; He, G.; Song, B.; Liu, D.; Xu, R. Early Paleozoic tectonic evolution of the Chinese South Tianshan Orogen: Constraints from SHRIMP zircon U–Pb geochronology and geochemistry of basaltic and dioritic rocks from Xiata, NW China. *Int. J. Earth Sci.* **2007**, *98*, 551–569. [[CrossRef](#)]
35. Han, B.F.; Guo, Z.J.; Zhang, Z.C.; Zhang, L.; Chen, J.F.; Song, B. Age, geochemistry, and tectonic implications of a late Paleozoic stitching pluton in the North Tian Shan suture zone, western China. *Geol. Soc. Am. Bull.* **2009**, *122*, 627–640. [[CrossRef](#)]
36. Feng, W.; Zhu, Y. Petrology and geochemistry of mafic and ultramafic rocks in the north Tianshan ophiolite: Implications for petrogenesis and tectonic setting. *Lithos* **2018**, *318–319*, 124–142. [[CrossRef](#)]
37. Xu, X.; Li, X.; Ma, Z.; Xia, L.; Xia, Z.; Peng, S. LA-ICPMS zircon U–Pb dating of gabbro from the Bayingou ophiolite in the northern Tianshan Mountains. *Acta Geol. Sin.* **2006**, *8*, 1168–1176.
38. He, G.-Q.; Li, M.-S.; Han, B.-F. Geotectonic research of southwest Tianshan and its west adjacent area, China. *Xinjiang Geol.* **2001**, *19*, 7–11.
39. Han, Y.; Zhao, G.; Sun, M.; Eizenhöfer, P.R.; Hou, W.; Zhang, X.; Liu, Q.; Wang, B.; Liu, D.; Xu, B. Late Paleozoic subduction and collision processes during the amalgamation of the Central Asian Orogenic Belt along the South Tianshan suture zone. *Lithos* **2016**, *246–247*, 1–12. [[CrossRef](#)]

40. Hegner, E.; Klemm, R.; Kroner, A.; Corsini, M.; Alexeiev, D.V.; Iaccheri, L.M.; Zack, T.; Dulski, P.; Xia, X.; Windley, B.F. Mineral ages and P-T conditions of Late Paleozoic high-pressure eclogite and provenance of melange sediments from Atbashi in the south Tianshan orogen of Kyrgyzstan. *Am. J. Sci.* **2011**, *310*, 916–950. [[CrossRef](#)]
41. Zhang, L.; Ai, Y.; Li, X.; Rubatto, D.; Song, B.; Williams, S.; Song, S.; Ellis, D.; Liou, J.G. Triassic collision of western Tianshan orogenic belt, China: Evidence from SHRIMP U–Pb dating of zircon from HP/UHP eclogitic rocks. *Lithos* **2007**, *96*, 266–280. [[CrossRef](#)]
42. Long, L.; Gao, J.; Klemm, R.; Beier, C.; Qian, Q.; Zhang, X.; Wang, J.; Jiang, T. Geochemical and geochronological studies of granitoid rocks from the Western Tianshan Orogen: Implications for continental growth in the southwestern Central Asian Orogenic Belt. *Lithos* **2011**, *126*, 321–340. [[CrossRef](#)]
43. Zhang, L.; Du, J.; Lü, Z.; Yang, X.; Gou, L.; Xia, B.; Chen, Z.; Wei, C.; Song, S. A huge oceanic-type UHP metamorphic belt in southwestern Tianshan, China: Peak metamorphic age and P-T path. *Chin. Sci. Bull.* **2013**, *58*, 4378–4383. [[CrossRef](#)]
44. Dong, Y.; Zhang, G.; Neubauer, F.; Liu, X.; Hauzenberger, C.; Zhou, D.; Li, W. Syn- and post-collisional granitoids in the Central Tianshan orogen: Geochemistry, geochronology and implications for tectonic evolution. *Gondwana Res.* **2011**, *20*, 568–581. [[CrossRef](#)]
45. Gao, J.; Wang, X.-S.; Klemm, R.; Jiang, T.; Qian, Q.; Mu, L.-X.; Ma, Y.-Z. Record of assembly and breakup of Rodinia in the Southwestern Altaids: Evidence from Neoproterozoic magmatism in the Chinese Western Tianshan Orogen. *J. Asian Earth Sci.* **2015**, *113*, 173–193. [[CrossRef](#)]
46. Hu, A.-Q.; Wei, G.-J.; Jiang, B.-M.; Zhang, J.-B.; Deng, W.-F.; Chen, L.-L. Formation of the 0.9 Ga Neoproterozoic granitoids in the Tianshan Orogen, NW China: Constraints from the SHRIMP zircon age determination and its tectonic significance. *Geochimica* **2010**, *39*, 197–212. [[CrossRef](#)]
47. Wang, X.-S.; Klemm, R.; Gao, J.; Jiang, T. Three episodes of Precambrian mafic magmatism in the southern Central Tianshan Block (NW China): Insight into an evolving geodynamic model. *Precambrian Res.* **2020**, *351*, 105961. [[CrossRef](#)]
48. Gou, L.-L.; Zhang, L.-F.; Lü, Z.; Shen, T.-T. Geochemistry and geochronology of S-type granites and their coeval MP/HT meta-sedimentary rocks in Chinese Southwest Tianshan and their tectonic implications. *J. Asian Earth Sci.* **2015**, *107*, 151–171. [[CrossRef](#)]
49. Yang, S.-H.; Zhou, M.-F. Geochemistry of the ~430-Ma Jingbulake mafic–ultramafic intrusion in Western Xinjiang, NW China: Implications for subduction related magmatism in the South Tianshan orogenic belt. *Lithos* **2009**, *113*, 259–273. [[CrossRef](#)]
50. Xu, X.-Y.; Wang, H.-L.; Li, P.; Chen, J.-L.; Ma, Z.-P.; Zhu, T.; Wang, N.; Dong, Y.-P. Geochemistry and geochronology of Paleozoic intrusions in the Nalati (Narati) area in western Tianshan, Xinjiang, China: Implications for Paleozoic tectonic evolution. *J. Asian Earth Sci.* **2013**, *72*, 33–62. [[CrossRef](#)]
51. Wang, B.; Zhai, Y.; Kapp, P.; de Jong, K.; Zhong, L.; Liu, H.; Ma, Y.; Gong, H.; Geng, H. Accretionary tectonics of back-arc oceanic basins in the South Tianshan: Insights from structural, geochronological, and geochemical studies of the Wuwamen ophiolite mélange. *GSA Bull.* **2017**, *130*, 284–306. [[CrossRef](#)]
52. Zhong, L.; Wang, B.; Shu, L.; Liu, H.; Mu, L.; Ma, Y.; Zhai, Y. Structural overprints of early Paleozoic arc-related intrusive rocks in the Chinese Central Tianshan: Implications for Paleozoic accretionary tectonics in SW Central Asian Orogenic Belts. *J. Asian Earth Sci.* **2015**, *113*, 194–217. [[CrossRef](#)]
53. Zhang, L.; Lü, Z.; Zhang, G.; Song, S. The geological characteristics of oceanic-type UHP metamorphic belts and their tectonic implications: Case studies from Southwest Tianshan and North Qaidam in NW China. *Sci. Bull.* **2008**, *53*, 3120–3130. [[CrossRef](#)]
54. Li, J.-L.; Klemm, R.; Gao, J.; Jiang, T.; Song, Y.-H. A common high-pressure metamorphic evolution of interlayered eclogites and metasediments from the ‘ultrahigh-pressure unit’ of the Tianshan metamorphic belt in China. *Lithos* **2015**, *226*, 169–182. [[CrossRef](#)]
55. Brey, G.P.; Köhler, T. Geothermobarometry in Four-phase Lherzolites II. New Thermobarometers, and Practical Assessment of Existing Thermobarometers. *J. Petrol.* **1990**, *31*, 1353–1378. [[CrossRef](#)]
56. Wells, P.R.A. Pyroxene Thermometry in Simple and Complex Systems. *Contr. Miner. Pet.* **1977**, *62*, 129–139. [[CrossRef](#)]
57. Wood, B.J.; Banno, S. Garnet-Orthopyroxene and Orthopyroxene-Clinopyroxene Relationships in Simple and Complex Systems. *Contr. Miner. Pet.* **1973**, *42*, 109–124. [[CrossRef](#)]
58. Wei, C.; Guan, X.; Dong, J. HT-UHT metamorphism of metabasites and the petrogenesis of TTGs. *Acta Petrol. Sin.* **2017**, *33*, 1381–1404.
59. Anderson, J.L.; Smith, D.R. The effects of temperature and f_{O_2} on the Al-in-hornblende barometer. *Am. Mineral.* **1995**, *80*, 549–559. [[CrossRef](#)]
60. Hammarstrom, J.M.; Zen, E.A. Aluminum in hornblende: An empirical igneous geobarometer. *Am. Mineral.* **1986**, *71*, 1297–1313.
61. Schmidt, M.W. Amphibole composition in tonalite as a function of pressure: An experimental calibration of the Al-in-hornblende barometer. *Contrib. Miner. Pet.* **1992**, *110*, 304–310. [[CrossRef](#)]

Disclaimer/Publisher’s Note: The statements, opinions and data contained in all publications are solely those of the individual author(s) and contributor(s) and not of MDPI and/or the editor(s). MDPI and/or the editor(s) disclaim responsibility for any injury to people or property resulting from any ideas, methods, instructions or products referred to in the content.